Click Here
for
Full Article

Inertial-range anisotropies in the solar wind from 0.3 to 1 AU: Helios 1 observations

Benjamin T. MacBride,[1] Charles W. Smith,[1] and Bernard J. Vasquez[1]

[1] In this study we analyze the evolution of solar wind turbulence from 0.3 to 1 AU using a database of 387 intervals from the Helios 1 spacecraft. Our results uphold the conclusion made by Smith et al. (2006), who used data from 1 AU, that the magnetic variance anisotropy scales with both proton beta and the amplitude of fluctuations in the power spectrum all the way down to 0.3 AU. We confirm the result of Bieber et al. (1996) that ~80% of the energy is contained in the wave vectors perpendicular to the mean magnetic field and in light of Dasso et al. (2005) we compute the fraction of energy in field-aligned wave vectors for high- and low-speed intervals separately. As Hamilton et al. found at 1 AU, we also see no clear reliance of the energy contained in parallel and perpendicular wave vectors based on wind speed at any heliocentric distance between 0.3 and 1 AU in the range of frequencies we study (5 to 20 mHz). These results combine to tell the story that the turbulent properties of the solar wind we analyze are fully consistent with the 1 AU observations and no discernable evolution can be found.

Citation: MacBride, B. T., C. W. Smith, and B. J. Vasquez (2010), Inertial-range anisotropies in the solar wind from 0.3 to 1 AU: Helios 1 observations, *J. Geophys. Res.*, *115*, A07105, doi:10.1029/2009JA014939.

1. Introduction

[2] Recent developments in the theory and observations of interplanetary turbulence lend strong support to the assertion that wave vectors nearly orthogonal to the mean magnetic field play an important role in the dynamics and evolution of the inertial range spectrum. *Matthaeus et al.* [1990] use rotations of the mean magnetic field and the computation of a universal correlation function for magnetic fluctuations to demonstrate that magnetic energy is preferentially distributed between field-aligned and perpendicular wave vectors. *Bieber et al.* [1996] provide a mechanism for computing the distribution of energy between field-aligned and perpendicular wave vectors in a turbulent magnetofluid that is applicable to single-spacecraft observations. Hereafter, we simply refer to this method as the "Bieber analysis." Using a database of 454 magnetic field data intervals recorded by the Helios spacecraft, each 34 min in duration and seen in association with 29 distinct solar energetic particle (SEP) events, they conclude that the perpendicular wave vectors contain ~80% of the energy while the field-aligned wave vectors contain only ~20% of the total magnetic energy at frequencies 0.98–20.5 mHz. *Dasso et al.* [2005] repeat the Matthaeus et al. analysis using five years of 64 s Advanced Composition Explorer (ACE) data from 1 AU and show that the fast (slow) wind preferentially populates the field-aligned (perpendicular) wave vectors. *Osman and Horbury* [2007] use multi-

spacecraft techniques to study the distribution of energy across wave vectors at smaller scales and in slow wind only, and they conclude that a significant 2-D component is required by the observations. The Matthaeus et al. analysis was a combination of wind speeds and there is a strong likelihood that the Bieber et al. analysis was as well.

[3] Underpinning these analyses is the question "To what extent are the observed spectra remnants of solar source and to what extent do in situ dynamics play a role in the formation of the spectral characteristics?" *Hamilton et al.* [2008] use ACE magnetic field data to argue that the large-scale fluctuations studied by *Dasso et al.* [2005] may be largely a remnant feature of the solar source. If true, the above division of energy into field-aligned wave vectors in fast winds and perpendicular wave vectors in slow winds is largely the result of the acceleration processes and perhaps the early solar wind evolution. Hamilton et al. find that at spacecraft frame frequencies > 10 mHz there is no difference in the distribution of energy according to wind speed. They further argue that this is because the lifetime of a turbulent fluctuation at these scales is short compared with the transit time of the solar wind so that the high-frequency fluctuations arise via in situ turbulent dynamics while the low-frequency fluctuations remain, to a greater degree, remnants of the acceleration process. If this is true, it is interesting to re-examine the evolution of the turbulence using Helios data in order to observe the possible evolution of fast and slow wind intervals.

[4] We focus here on the results of *Bieber et al.* [1996], *Leamon et al.* [1998a], *Smith et al.* [2006], and *Hamilton et al.* [2008] who studied properties of solar wind turbulence at 1 AU in the high frequency end of the inertial range. Smith et al. study the magnetic variance anisotropy (ratio of variance

---

[1]Physics Department and Space Science Center, University of New Hampshire, Durham, New Hampshire, USA.
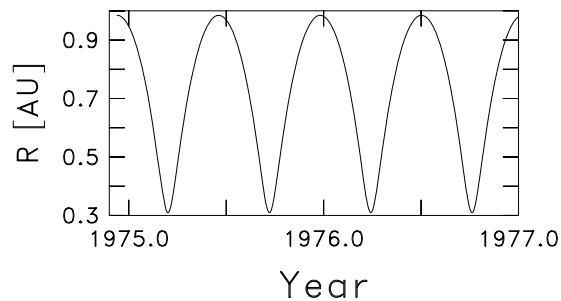
Figure 1. Heliocentric distance for Helios1 during years when data for this study was obtained.

Figure 2. Number of intervals selected for study in increments of 0.1 AU.

in the perpendicular fluctuations to the variance in the parallel fluctuations) and find it scales with both proton beta and the amplitude of the power spectrum. In their analysis they also plot proton beta against the amplitude of the power spectrum of magnetic field oscillations and find them to be correlated, which leads to the result that magnetic variance anisotropy scales with both quantities. Proton beta is a unitless quantity defined as the ratio of thermal to magnetic energy density, and if the variation of the magnetic field is related to the proton temperature [*Smith et al.*, 2006] it will be difficult to discern whether the anisotropy arises due to the variation of the proton beta or the amplitude of the power spectrum.

[5] *Bieber et al.* [1996], *Leamon et al.* [1998a], and *Hamilton et al.* [2008] study the wave vector anisotropy in the solar wind which gives an estimate of the relative energy contained in the fluctuation vectors perpendicular and parallel to the mean magnetic field. Leamon et al. apply the Bieber analysis to high-frequency observations in the inertial range at 1 AU and find 89% of the energy resides in wave vectors perpendicular to the mean magnetic field. Hamilton et al. use the same analysis in both the inertial and dissipation ranges at 1 AU but with an additional selection mechanism based on wind speed. Their results demonstrate that field-aligned wave vectors constitute ~30% of the total energy at inertial range scales with no significant dependence on wind speed.

[6] In this analysis we extend the methods that have been used previously at 1 AU to the inner heliosphere using observations by the Helios spacecraft. Additionally, we analyze the magnetic variance and wave vector anisotropies as a function of both wind speed and heliocentric distance. We attempt to determine whether or not there is an observed spatial evolution of the turbulent properties as a function of heliocentric distance and whether or not there is a distinction between fast and slow winds.

2. Database Construction

[7] In the analysis we use Helios 1 spacecraft magnetic field data with 6 s resolution from the years 1974 through 1977. The Helios spacecraft traversed an orbit with a perihelion of 0.3 AU and an aphelion of 1 AU, so the recorded data spans this spatial range. Figure 1 displays the heliocentric distance of the Helios spacecraft as a function of time from 1974 until 1977. We use 387 hand-selected intervals ranging from 4 to 6 h in length to create magnetic power spectra by a prewhitened *Blackman and Tukey* [1958] method based on the autocorrelation functions. Intervals are selected on the basis of apparent stationarity of their means and
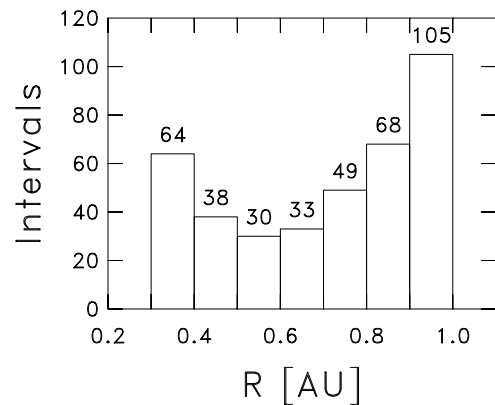
fluctuation levels in the hope of obtaining spectra that are applicable to homogeneous turbulence theory. Intervals with a well-defined power law index through the inertial range were kept, while a few intervals with poorly obtained power law spectra (most notably those containing negative energy as is a possibility with Blackman-Tukey analyses) were discarded. From the power spectra we analyze two frequency intervals in the inertial range (5 to 20 mHz and 30 to 70 mHz) which we refer to as the low-frequency and high-frequency intervals, respectively. Time intervals were chosen on the basis of providing a wide range of properties to analyze. In particular, we include intervals spanning 0.3 to 1 AU and spanning all available wind speeds. Figure 2 displays the number of intervals chosen as a function of distance from the Sun in increments of 0.1 AU and Figure 3 shows the distribution function of wind speeds for the events chosen. These two plots demonstrate a full coverage of the inner heliosphere from 0.3 to 1 AU and a range of wind speeds from 250 to 750 km/s.

2.1. IMF Spectra of Helios 1

[8] We obtained the data from the National Space Science Data Center (NSSDC) via COHOWEB and studied the documentation available. Figure 4 shows an example of the spectra computed in this study. The interval is from 1900 to 2300 UT on day 273 of 1975 when the spacecraft is at 0.37 AU. Solar wind conditions are $V_{SW} = 428$ km/s, $\beta_p = 0.04$,
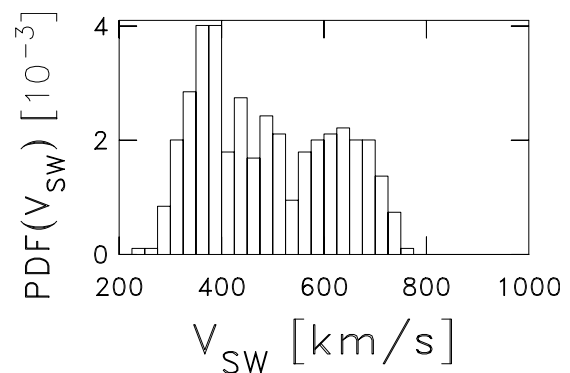

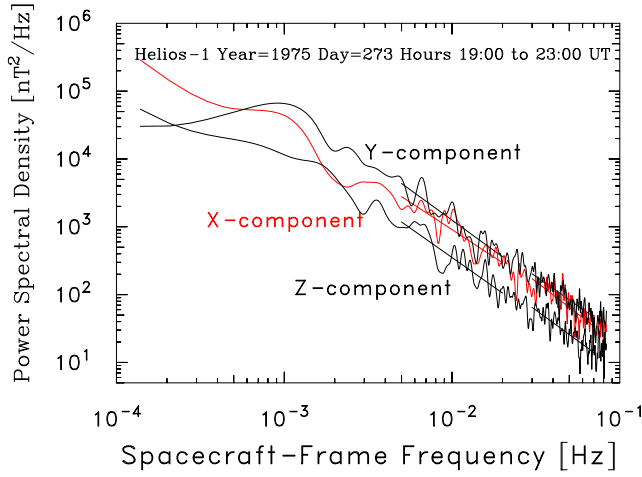**Figure 3.** Distribution function of events according to wind speed.

Figure 4. Example component power spectra for magnetic fluctuations at 0.3 AU.

and $\Theta_{BR} = 33°$. The data are rotated into mean field coordinates as defined by [*Bieber et al.*, 1996]:

$$\hat{\mathbf{e}}_{\mathbf{x}} \equiv (\hat{\mathbf{e}}_{\mathbf{R}} \times \hat{\mathbf{e}}_{\mathbf{B}})/|\hat{\mathbf{e}}_{\mathbf{R}} \times \hat{\mathbf{e}}_{\mathbf{B}}|, \tag{1}$$

$$\hat{\mathbf{e}}_{\mathbf{y}} \equiv \hat{\mathbf{e}}_{\mathbf{z}} \times \hat{\mathbf{e}}_{\mathbf{x}}, \tag{2}$$

$$\hat{\mathbf{e}}_{\mathbf{z}} \equiv \hat{\mathbf{e}}_{\mathbf{B}} \tag{3}$$

and spectra for each of the three components are computed. The two frequency intervals described above are fit by power law forms. Table 1 lists the computed spectral indexes. All spectra except the Y-component show evidence of spectral steepening in the high-frequency interval. This general behavior of spectral steepening is seen throughout our analysis of the Helios 1 data.

[9] We compute the mean and standard deviation for the power law index in each frequency interval over limited ranges of heliocentric distance and plot the results in Figure 5. In the process, we separate the samples for low-speed wind ($V_{SW} < 400$ km/s) and high-speed wind ($V_{SW} > 500$ km/s) as is done by *Dasso et al.* [2005]. Table 2 lists the values from Figure 5 including the number of samples in each subset and the computed error of the means which are important to the following arguments. The error of the means are small and comparable to or less than twice the size of the symbols used in the plot. The standard deviation of the samples is large, but still some trends emerge when one compares the changing means against the errors. There is an overall spectral steepening with increasing heliocentric distance as reported by *Bavassano et al.* [1982]. This is demonstrated by the

Table 1. Figure 4 Fit Parameters

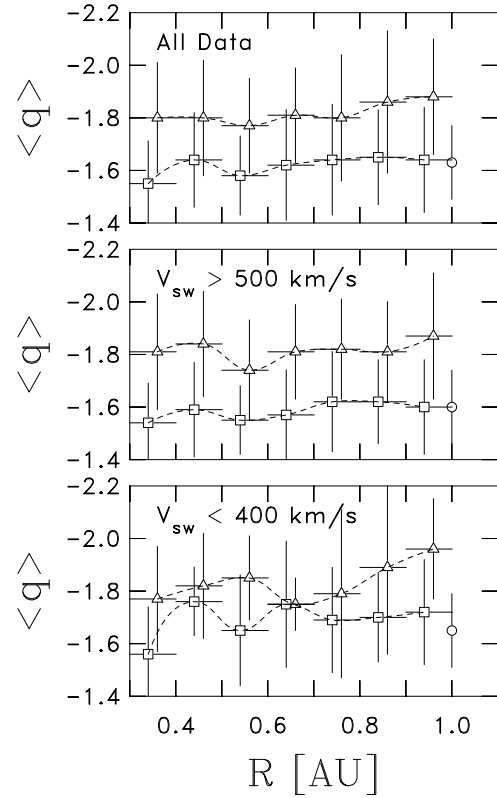| Component	Frequency Fit Intervals	
	5 to 20 mHz	30 to 70 mHz
X	−1.61 ± 0.06	−1.90 ± 0.06
Y	−1.80 ± 0.06	−1.74 ± 0.05
Z	−1.74 ± 0.07	−1.81 ± 0.06
Trace	−1.73 ± 0.05	−1.82 ± 0.04

Figure 5. Means and standard deviations of power law indexes for low-frequency range (squares) and high-frequency range (triangles) computed from all data (top), high-speed wind intervals (middle), and low-speed winds (bottom).

changing means that are greater than the error of the means, thereby demonstrating that the shift of the distribution is smaller than the width. Likewise, the average power law index for the slow solar wind is continually higher than in the fast solar wind by an amount considerably greater than the error of the mean. Note that the spectra in the high-frequency intervals consistently average to be steeper than in the low-frequency intervals and the former are inconsistent with ACE observations at 1 AU. The circular data point at the 1 AU value is a result drawn from *Hamilton et al.* [2008] in the range 10 to 100 mHz. Another problem is that the high-frequency fits are consistently steeper than 1 AU observations even at 0.3 AU.

[10] We have tested our codes and tested our results against independent analyses (R. Bruno, private communication, 2007) and we are forced to conclude that the measurements in the high-frequency range are not correct. We believe that either the instrument response function is not flat at these frequencies or the data was poorly filtered prior to deposition in the NSSDC. There is no apparent evidence of this problem with Helios 2 observations. For this reason we will continue this analysis using only the low-frequency results.

2.2. Analysis Techniques

[11] Once the spectral information is obtained, we are able to compare the computed parameters in search of correlations and trends. One quantity of interest is the variance anisotropy $\delta B_{\perp}^2/\delta B_{\parallel}^2$ where $\delta B_{\perp}^2 \equiv \delta B_x^2 + \delta B_y^2$ and $\delta B_{\parallel}^2 \equiv \delta B_z^2$ averaged

Table 2. Figure 5 Values

Wind Subset	Frequency Range, mHz	R AU	Number of Samples	$\langle q \rangle \pm \sigma$ (Standard Deviation)
All data	5–20	0.3–0.4	64	−1.55 ± 0.02 (0.16)
All data	5–20	0.4–0.5	38	−1.64 ± 0.03 (0.18)
All data	5–20	0.5–0.6	30	−1.58 ± 0.03 (0.15)
All data	5–20	0.6–0.7	33	−1.62 ± 0.04 (0.21)
All data	5–20	0.7–0.8	49	−1.64 ± 0.03 (0.21)
All data	5–20	0.8–0.9	68	−1.65 ± 0.02 (0.18)
All data	5–20	0.9–1.0	105	−1.64 ± 0.02 (0.20)
All data	30–70	0.3–0.4	64	−1.80 ± 0.03 (0.21)
All data	30–70	0.4–0.5	38	−1.80 ± 0.04 (0.22)
All data	30–70	0.5–0.6	30	−1.77 ± 0.03 (0.18)
All data	30–70	0.6–0.7	33	−1.81 ± 0.03 (0.18)
All data	30–70	0.7–0.8	49	−1.80 ± 0.03 (0.24)
All data	30–70	0.8–0.9	68	−1.86 ± 0.03 (0.27)
All data	30–70	0.9–1.0	105	−1.88 ± 0.02 (0.22)
Fast wind	5–20	0.3–0.4	18	−1.54 ± 0.04 (0.15)
Fast wind	5–20	0.4–0.5	24	−1.59 ± 0.04 (0.18)
Fast wind	5–20	0.5–0.6	15	−1.55 ± 0.03 (0.13)
Fast wind	5–20	0.6–0.7	22	−1.57 ± 0.04 (0.17)
Fast wind	5–20	0.7–0.8	18	−1.62 ± 0.04 (0.19)
Fast wind	5–20	0.8–0.9	22	−1.62 ± 0.03 (0.16)
Fast wind	5–20	0.9–1.0	49	−1.60 ± 0.03 (0.18)
Fast wind	30–70	0.3–0.4	18	−1.81 ± 0.05 (0.22)
Fast wind	30–70	0.4–0.5	24	−1.84 ± 0.04 (0.20)
Fast wind	30–70	0.5–0.6	15	−1.74 ± 0.05 (0.19)
Fast wind	30–70	0.6–0.7	22	−1.81 ± 0.04 (0.18)
Fast wind	30–70	0.7–0.8	18	−1.82 ± 0.04 (0.19)
Fast wind	30–70	0.8–0.9	22	−1.81 ± 0.04 (0.19)
Fast wind	30–70	0.9–1.0	49	−1.87 ± 0.03 (0.24)
Slow wind	5–20	0.3–0.4	35	−1.56 ± 0.03 (0.18)
Slow wind	5–20	0.4–0.5	9	−1.76 ± 0.04 (0.13)
Slow wind	5–20	0.5–0.6	8	−1.65 ± 0.07 (0.21)
Slow wind	5–20	0.6–0.7	8	−1.76 ± 0.08 (0.24)
Slow wind	5–20	0.7–0.8	17	−1.69 ± 0.05 (0.20)
Slow wind	5–20	0.8–0.9	33	−1.70 ± 0.03 (0.17)
Slow wind	5–20	0.9–1.0	22	−1.72 ± 0.04 (0.20)
Slow wind	30–70	0.3–0.4	35	−1.77 ± 0.03 (0.20)
Slow wind	30–70	0.4–0.5	9	−1.82 ± 0.07 (0.20)
Slow wind	30–70	0.5–0.6	8	−1.85 ± 0.06 (0.16)
Slow wind	30–70	0.6–0.7	8	−1.75 ± 0.04 (0.10)
Slow wind	30–70	0.7–0.8	17	−1.79 ± 0.08 (0.32)
Slow wind	30–70	0.8–0.9	33	−1.89 ± 0.06 (0.33)
Slow wind	30–70	0.9–1.0	22	−1.96 ± 0.04 (0.19)

over the prescribed frequency range. We use δB to represent the fluctuation relative to the mean field while subscripts $\parallel$ and $\perp$ are defined relative to the mean field direction. This is analogous to the *Belcher and Davis* [1971] analysis which found an anisotropy of 9 in the trailing edge of high-speed streams. The computed variance anisotropy for the example spectra shown in Figure 4 is 6.7 ± 2.6 for the low-frequency interval.

[12] While there are other quantities obtainable in similar fashion, the other of prime interest here is the wave vector anisotropy as measured by the technique of *Bieber et al.* [1996]. *Leamon et al.* [1998a] and *Hamilton et al.* [2008] present reviews of this method and we describe it only briefly here. Bieber et al. argue that (1) if the multidimensional correlation function is locally axisymmetric in the expanding flow, which assumes that the spectral energy distribution is oriented only by the mean magnetic field and attempting to maintain axisymmetry faster than expansion will distort the correlation function; (2) if the energy is divided between wave vectors parallel and perpendicular to the mean field only; and (3) if both spectra have the same power law index, then it is possible to use the two perpendicular component spectra to compute the division of energy

between the parallel and perpendicular wave vectors. We know of no independent measurement of the axisymmetry assumption derived from a single or multiple spacecraft now available, although multiple spacecraft techniques could resolve the issue with sufficient data. Bieber et al. derive:

$$\frac{P_{yy}}{P_{xx}} = \frac{k_s^{1-|q|} + r'\left(\frac{2|q|}{1+|q|}\right)k_2^{1-|q|}}{k_s^{1-|q|} + r'\left(\frac{2}{1+|q|}\right)k_2^{1-|q|}} \qquad (4)$$

where

$$k_2 = \frac{2\pi\nu}{V_{sw}\sin\Theta_{BR}} \qquad (5)$$

$$k_s = \frac{2\pi\nu}{V_{sw}\cos\Theta_{BR}} \qquad (6)$$

are the 2-D and field-aligned wave vectors with projections at spacecraft frame frequency ν, P_{xx} and P_{yy} are the measured power spectra in the mean field coordinates described above, q is the power law index of the spectrum (always found to be
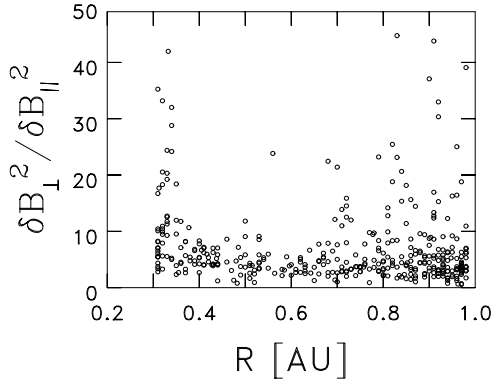
Figure 6. Scatterplot of variance anisotropy for low-frequency range (side axis) versus heliocentric distance for all data.

Figure 7. Scatterplot of variance anisotropy for low-frequency range (side axis) versus thermal proton β_p for all data.

negative), Θ_{BR} is the angle between the mean field and the solar wind flow, and $r' = C_2/C_s$ is the ratio of energy in the 2-D component C_2 and field-aligned (slab) component C_s. (Note that *Hamilton et al.* [2008] misprint equations (5) and (6) as well as the definition of r'.) It is then possible to write:

$$r' = [\tan \Theta_{BR}]^{1-|q|} \left\{ \frac{\frac{P_{yy}}{P_{xx}} - 1}{|q| - \frac{P_{yy}}{P_{xx}}} \right\} \left(\frac{1 + |q|}{2} \right) \qquad (7)$$

and

$$r = \frac{C_s}{C_s + C_2}$$
$$= \frac{1}{1 + r'} \qquad (8)$$

where r is the fraction of energy associated with the field-aligned wave vectors within the prescribed frequency band. There are two ways to apply this formalism: Either P_{yy}/P_{xx} can be binned into intervals of Θ_{BR} and the resulting relationship fit with equation (4) to determine r, or r can be computed from each data interval using equations (7) and (8) and then averaged. The former has the advantage of verifying the above relationship. The latter benefits from better statistics. We perform both methods in this paper to determine the fraction of energy contained in the field-aligned and perpendicular wave vectors. When computing the weighted average value of r, we have adopted a floor value of uncertainty of 0.1. Therefore we set the uncertainty to be 0.1 for those few points with smaller calculated uncertainty. In the case of the example spectra shown in Figure 4 the computed value of P_{yy}/P_{xx} for the low-frequency interval is 1.4 ± 0.5. The computed value of $\Theta_{BR} = 33°$. The large uncertainty in the spectral ratio for this event results in $r = 28 \pm 52\%$.

3. Variance Anisotropy

[13] As stated in section 1, *Smith et al.* [2006] found the magnetic variance anisotropy to scale with both proton beta (β_p) and the amplitude of the spectrum of magnetic fluctuations ($\delta B/B_0$). This result was the product of an analysis based on measurements taken with the ACE spacecraft at 1 AU and we seek to extend this analysis to the inner heliosphere with the Helios spacecraft.
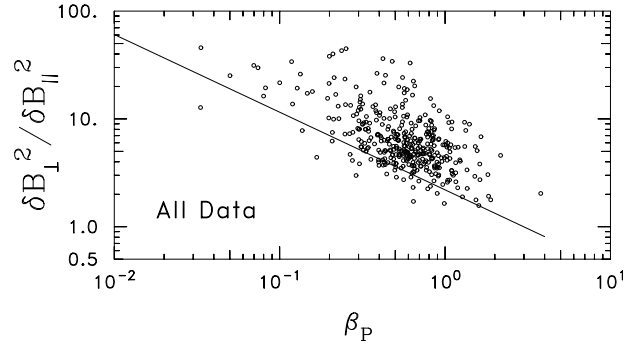
[14] Figure 6 shows the computed variance anisotropy for the low-frequency range plotted as a function of heliocentric distance. Note that no clear dependence is seen. While this could be the result of the data interval selection wherein the same conditions were not chosen at both 0.3 and 1 AU, the following plots suggest an alternate interpretation.

[15] Figure 7 plots the magnetic variance anisotropy of the low frequency range versus β_p. This plot is created using all of the intervals that we analyzed with no selection based on heliocentric distance or wind speed. As in the case of *Smith et al.* [2006] we again find the variance anisotropy to scale with β_p. Figure 8 plots the magnetic variance anisotropy of the low-frequency range against $\delta B/B_0$, the square root of the integrated power in the fit frequency range normalized by the mean field intensity. Figure 8 (top) uses all 387 intervals from the Helios database while Figure 8 (bottom) uses only the 64 intervals in our database recorded by Helios when the spacecraft was in the 0.3 to 0.4 AU range. Both results show a
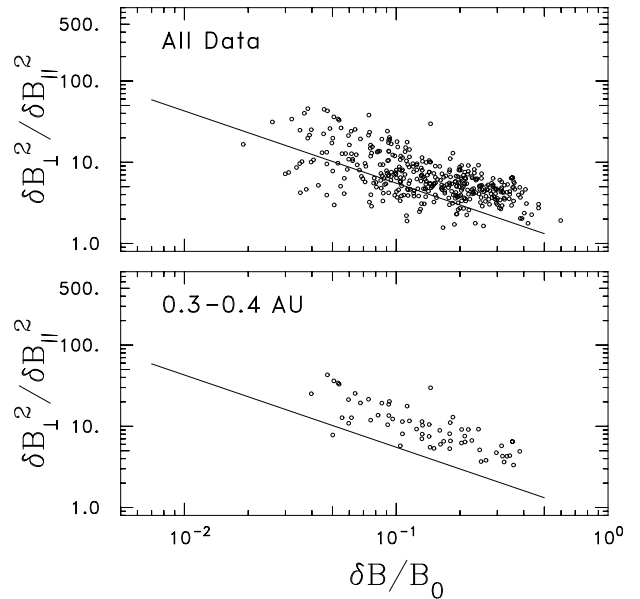

Figure 8. (top) Scatterplot of variance anisotropy for low-frequency range (side axis) versus integrated magnetic power normalized to mean field intensity (bottom axis) for all data. (bottom) Same for heliocentric distance range 0.3–0.4 AU.
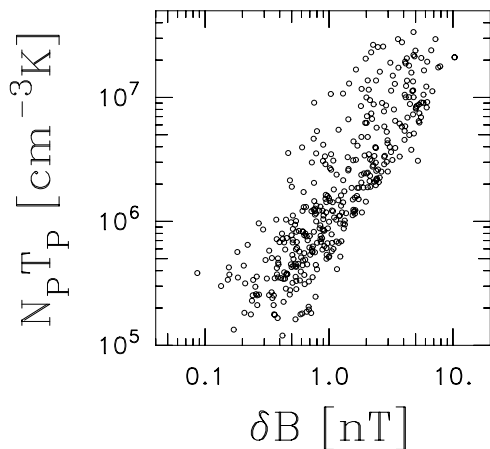
Figure 9. Scatterplot of proton thermal energy (side axis) versus integrated magnetic fluctuation amplitude (bottom axis) for all data.

[18] Here we employ the Bieber test described in section 2.2 to examine the dependence of wave vector anisotropy on not only wind speed as demonstrated by *Hamilton et al.* [2008] but also on heliocentric distance from 0.3 to 1 AU. By using data from the Helios spacecraft we have the opportunity to compare the percentage of energy contained in the wave vectors perpendicular and parallel to the mean field at various locations in the inner heliosphere. By comparing results at different heliocentric distances it is possible to determine whether the wave vector anisotropy evolves as the solar wind expands from its solar source. Figure 10 displays the ratio of power in the two components perpendicular to the mean field as a function of the angle between the mean field
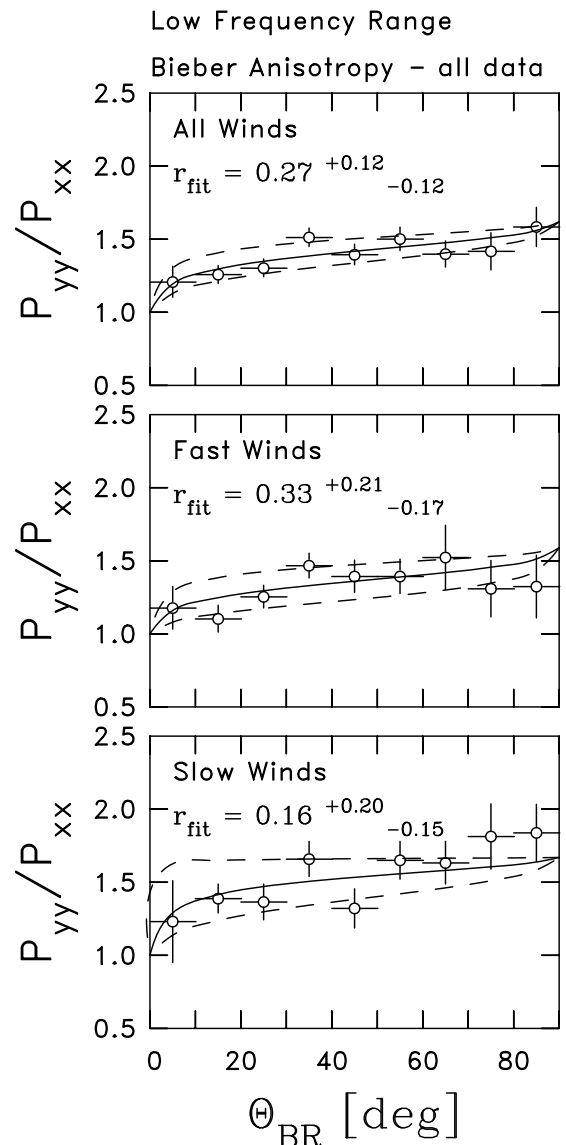
scaling of the variance anisotropy with $\delta B/B_0$. This is also in accordance with the Smith et al. results at 1 AU. In fact, the trend lines shown in Figures 7 and 8 are the same lines used in the analysis at 1 AU. These results suggest that the magnetic variance anisotropy experiences no spatial evolution between 0.3 and 1 AU apart from its dependence on in situ variables.

[16] Similar to the results of *Smith et al.* [2006], we find a dependence of the magnetic variance anisotropy on both β_p and $\delta B/B_0$. Prior to the analysis we thought taking samples from varying heliocentric distances might break the correlation between the dependence on both β_p and $\delta B/B_0$ to determine which quantity is fundamental to the variance anisotropy, but this did not happen. The variance anisotropy scales with both quantities all the way down to 0.3 AU. Figure 9 plots the thermal energy of the protons in the solar wind against the amplitude of the power spectra and they are shown to be correlated as reported by *Grappin et al.* [1990]. This correlation is what leads the magnetic variance anisotropy to scale with both parameters in Figure 9.

4. Wave Vector Anisotropy

[17] As stated in section 1, the test to determine the orientation of the wave vectors in solar wind turbulence was developed by *Bieber et al.* [1996], and its first application used data from SEP events observed by the Helios spacecraft. That analysis focused on the frequency range 0.1 to 20 mHz and showed that ~80% of the energy resides in the 2-D component perpendicular to the mean magnetic field. *Leamon et al.* [1998a] applied the Bieber test to data taken at 1 AU by the WIND spacecraft and found 89% of the energy residing in 2-D component over the frequency range 10 to 200 mHz. *Hamilton et al.* [2008] employed this same test using data from the ACE spacecraft with inertial range frequencies 8 to 100 mHz and found ~70% 2-D. Furthermore, Hamilton et al. selected events based on the average flow speed of the solar wind for each interval and found no distinction in wave vector orientation between the intervals with high-speed (V_{SW} > 500 km/s) and low-speed (V_{SW} < 400 km/s) streams.

Figure 10. (top) Distribution of computed ratio P_{yy}/P_{xx} for low-frequency fits binned by Θ_{BV} for all low-frequency data. Minimum χ_r^2 solution (solid line) and $\chi_r^2 + 1$ curves (dashed lines) are shown. (middle) Same for all fast wind data. (bottom) Same for all slow wind data. Top to bottom, best-fit values of χ_r are 0.64, 0.72, and 0.62.

Table 3. Field-Aligned Fractions

Component	Fit	Average
All data	0.27^{+12}_{-12}	0.25 ± 0.02
Fast winds	0.33^{+21}_{-17}	0.30 ± 0.05
Slow winds	0.16^{+20}_{-15}	0.25 ± 0.04

and the solar wind flow direction Θ_{BR}. The minimum χ^2 fit of the function in equation (4) to this data gives an estimate of the percentage of energy contained in the field-aligned wave vector. We find $27^{+12}_{-12}\%$ of the energy is contained in the field-aligned wave vectors using all of the data ranging from heliocentric distances of 0.3 to 1 AU with no selection based on wind speed. Performing the analysis with a filter for average solar wind speed for an interval yields a field-aligned fraction of $16^{+20}_{-15}\%$ and $33^{+21}_{-17}\%$ for the low-speed and high-speed wind, respectively.

[19] Table 3 lists the fraction of energy contained in the wave vectors aligned with the mean magnetic field computed from equations (7) and (8). The average value with no wind speed selection is $25\% \pm 2\%$, and $25\% \pm 4\%$ and $30\% \pm 5\%$ for slow and fast wind intervals, respectively. These average values of the field-aligned fraction agree with those computed from the fit of equation (4) to measured values of P_{yy}/P_{xx} for different values of θ_{BR}. Furthermore, the average and fit values for the field-aligned fraction for low-speed intervals lie within the uncertainty range for the average and fit values for the same quantity in high-speed intervals, and reverse is also true making the geometry of the fast and slow winds equivalent at these scales. The average and fit values for the analysis with no speed selection is also within the uncertainty ranges of the average and fit values for both the high-speed and low-speed analyses. These values are all within the uncertainty range of the field-aligned fraction computed by *Bieber et al.* [1996] of $27^{+7}_{-6}\%$ who also used data from the Helios spacecraft, albeit selectively using data around SEP events. Performing the same analysis with an additional filter based on heliocentric distance shows no statistically significant spatial evolution of the energy contained in the parallel and perpendicular wave vectors.

5. Discussion

[20] The independence of field-aligned fraction based on solar wind speed that we find in our results is contrary to the conclusions of *Dasso et al.* [2005]. Similar to the results of this analysis, *Hamilton et al.* [2008] also selected events based on the average flow speed of each interval and show no dependence of wave vector anisotropy on the solar wind speed. Hamilton et al. provide a resolution to these seemingly contradictory results. The resolution lies in the difference of frequencies used for the two analyses. Hamilton et al. show that $f_{sc} > 10$ mHz represents fluctuations that are too short-lived to be of solar origin and this holds down to the scope of the present analysis at 0.3 AU. All of our results arise from $f_{sc} > 1$ mHz. Hamilton et al. suggest that the distinction between slow and fast winds found by Dasso et al. could be a remnant of the solar source.

[21] Our inability to find a well-defined dependence of wave vector anisotropy on heliocentric distance is possibly the product of an insufficient amount of data combined with the apparent corruption of the high-frequency intervals ini-

tially prepared for this study. Although we include 387 total events in the entire analysis, once we begin selecting for wind speed along with spatial ranges in the heliosphere the number of events included to compute the average or fit the field-aligned fraction diminishes and the uncertainty of the average increases greatly. The average value of r computed at different heliocentric distances shows no correlation with the spatial location. In order to achieve statistically significant results for an analysis evaluating the dependence of the percentage of energy contained in parallel and perpendicular wave vectors on the heliocentric distance, many more intervals need to be added to the database.

6. Summary

[22] In this analysis we extend the findings of *Leamon et al.* [1998a], *Smith et al.* [2006], and *Hamilton et al.* [2008] to 0.3 AU and expand the results of *Bieber et al.* [1996] to include a division of the intervals into fast and slow wind categories. We extend the previous results based on observations made by the ACE and WIND spacecraft to observations made by Helios 1 in an attempt to determine whether or not the properties of solar wind turbulence experience a spatial evolution between 0.3 and 1 AU. We have confirmed the results of Smith et al. made at 1 AU that the magnetic variance anisotropy scales with both proton beta and the amplitude of the power spectrum. Similar to their results, we are unable to break the correlation between the proton beta and the amplitude of the power spectrum. These results hold down to 0.3 AU, the closest to the Sun that Helios travels. Bieber et al. found 26% of the energy resides in wave vectors aligned with the mean magnetic field, and from two independent analyses we find 27% and 25% of the energy to be in the field-aligned wave vectors, generally. Hamilton et al. found the wave vector anisotropy at 1 AU in the high frequency end of the inertial range to be independent of solar wind speed. We also analyze frequencies approaching the end of the inertial range, but this analysis is not restricted to measurements made at 1 AU; instead, it includes measurements made in the range of 0.3 to 1 AU. We also find the wave vector anisotropy to be independent of solar wind speed. In addition, we find that there is no discernable dependence of the wave vector anisotropy on heliocentric distance in the frequency range 5–20 mHz. These results of the magnetic variance and wave vector anisotropies that were made using data from the Helios spacecraft demonstrate that the high-frequency inertial-range turbulence measured at 0.3 AU is nearly identical to the observations at 1 AU.

References

Bavassano, B., M. Dobrowolny, F. Mariani, and N. F. Ness (1982), Radial evolution of power spectra of interplanetary Alfvénic turbulence, *J. Geophys. Res.*, *87*, 3617–3622.

Belcher, J. W., and L. Davis Jr. (1971), Large-amplitude Alfvén waves in the interplanetary medium, 2, *J. Geophys. Res.*, *76*, 3534–3563.

Bieber, J. W., W. H. Matthaeus, C. W. Smith, W. Wanner, M.-B. Kallenrode, and G. Wibberenz (1994), Proton and electron mean free paths: The Palmer consensus revisited, *Astrophys. J.*, *420*, 294–306.

Bieber, J. W., W. Wanner, and W. H. Matthaeus (1996), Dominant two-dimensional solar wind turbulence with implications for cosmic ray transport, *J. Geophys. Res.*, *101*, 2511–2522.

Dasso, S., L. J. Milano, W. H. Matthaeus, and C. W. Smith (2005), Anisotropy in fast and slow solar wind fluctuations, *Astrophys. J. Lett.*, *635*, L181–L184.

Freeman, J. W. (1998), Estimates of solar wind heating inside 0.3 AU, *Geophys. Res. Lett.*, *15*, 88–91.

Grappin, R., A. Mangeney, and E. Marsch (1990), On the origin of solar wind MHD turbulence: Helios data revisited, *J. Geophys. Res.*, *95*, 8197–8209.

Hamilton, K., C. W. Smith, B. J. Vasquez, and R. J. Leamon (2008), Inertial- and dissipation-range anisotropies in the solar wind at 1 AU, *J. Geophys. Res.*, *113*, A01106, doi:10.1029/2007JA012559.

Horbury, T. S., M. A. Forman, and S. Oughton (2005), Spacecraft observations of solar wind turbulence: An overview, *Plasma Phys. Control. Fusion*, *47*, B703–B717.

Kolmogorov, A. N. (1941), The local structure of turbulence in incompressible viscous fluid for very large Reynolds numbers, *Dokl. Akad. Nauk SSSR*, *30*, 301–305. (Reprinted in Proc. R. Soc. London A, 434, 9–13, 1991.)

Kraichnan, R. H. (1965), Inertial range of hydromagnetic turbulence, *Phys. Fluids*, *8*, 1385–1387.

Leamon, R. J., C. W. Smith, N. F. Ness, W. H. Matthaeus, and H. K. Wong (1998a), Observational constraints on the dynamics of the interplanetary magnetic field dissipation range, *J. Geophys. Res.*, *103*, 4775–4787.

Leamon, R. J., C. W. Smith, and N. F. Ness (1998b), Characteristics of magnetic fluctuations within coronal mass ejections: The January 1997 event, *Geophys. Res. Lett.*, *25*, 2505–2509.

Leamon, R. J., W. H. Matthaeus, C. W. Smith, and H. K. Wong (1998c), Contribution of cyclotron-resonant damping to kinetic dissipation of interplanetary turbulence, *Astrophys. J. Lett.*, *507*, L181–L184.

Leamon, R. J., C. W. Smith, N. F. Ness, and H. K. Wong (1999), Dissipation range dynamics: Kinetic Alfvén waves and the importance of β_e, *J. Geophys. Res.*, *104*, 22,331–22,344.

Leamon, R. J., W. H. Matthaeus, C. W. Smith, G. P. Zank, D. J. Mullan, and S. Oughton (2000), MHD driven kinetic dissipation in the solar wind and corona, *Astrophys. J.*, *537*, 1054–1062.

Matthaeus, W. H., M. L. Goldstein, and D. A. Roberts (1990), Evidence for the presence of quasi-two-dimensional nearly incompressible fluctuations in the solar wind, *J. Geophys. Res.*, *95*, 20,673–20,683.

McComas, D. J., S. J. Bame, P. Barker, W. C. Feldman, J. L. Phillips, P. Riley, and J. W. Griffee (1998), Solar wind electron proton alpha monitor (SWEPAM) for the Advanced Composition Explorer, *Space Sci. Rev.*, *86* (1–4), 563–612.

Osman, K. T., and T. S. Horbury (2007), Multispacecraft measurement of anisotropic correlation functions in solar wind turbulence, *Astrophys. J. Lett.*, *654*, L103–L106.

Smith, C. W., M. H. Acuña, L. F. Burlaga, J. L'Heureux, N. F. Ness, and J. Scheifele (1998), The ACE magnetic field experiment, *Space Sci. Rev.*, *86*(1–4), 613–632.

Smith, C. W., D. J. Mullan, N. F. Ness, R. M. Skoug, and J. Steinberg (2001), Day the solar wind almost disappeared: Magnetic field fluctuations, wave refraction, and dissipation, *J. Geophys. Res.*, *106*, 18,625–18,634.

Smith, C. W., D. J. Mullan, and N. F. Ness (2004), Further evidence of wave refraction associated with extended rarefaction events in the solar wind, *J. Geophys. Res.*, *109*, A01111, doi:10.1029/2003JA010113.

Smith, C. W., B. J. Vasquez, and K. Hamilton (2006), Interplanetary magnetic fluctuation anisotropy in the inertial range, *J. Geophys. Res.*, *111*, A09111, doi:10.1029/2006JA011651.

Wanner, W. (1993), Solar energetic proton scattering and the spatial structure of magnetic field turbulence in the inner heliosphere, Ph.D. thesis, Univ. of Kiel, Kiel, Germany.

———————
B. T. MacBride, C. W. Smith, and B. J. Vasquez, Space Science Center, Morse Hall, University of New Hampshire, Durham, NH 03824, USA. (Ben.MacBride@gmail.com; Charles.Smith@unh.edu; Bernie.Vasquez@unh.edu)